ME104 Project 4 Report, Team ” ”

Nick Abram, Rio Hall-Zazueta, Andrew Zerbe

Fig. 1. Top: Andrew’s robot, Bottom Left: Rio’s Robot, Bottom Center: Nick’s Robot, Bottom Left: Underside of Chassis

I. Robot Design

Our robot consists of a single driven wheel at its front, driven by a four-stage Tamiya planetary gearbox connected to a two-stage custom spur gearbox, and two caster wheels in the back. The chassis has a roughly triangular shape, motivated by the three contact points with the ground. A platform is attached to the chassis atop six custom 'pillars.' Weights were placed on the platform to ensure that the driven wheel would roll with minimal slipping.

The gearbox consists of involute spur gears, which were chosen due to their relatively high efficiency as well as their ease of design and manufacture. A test gearbox was created to estimate the efficiency of these gears. Further details can be found in Section III.

A two-stage reduction was ultimately specified, which required that the second and third gears, as well as the fourth gear and the wheel, rotate together. Each of these sets of two parts were printed as one component to avoid torque transmission through shafts, which would easily slip given the hardware we had available, and improve gear tooth strength. The first custom printed gear was secured directly to the output shaft of the motor gearbox, which was thick enough to support a cantilever load. The middle gears and the wheel were friction fit onto shafts and simply supported by bearings embedded in parallel walls of the gearbox. Further details about the wheel gear and the middle gears can be found in Section V & VI respectively. The bearings were placed in the walls as opposed to the gears to reduce the force multipliers at these connection points. The motor and its gearbox were mounted on the chassis using the included brackets, machine screws, and nuts, to reduce vibration in the gear. The custom gearbox was fit into a cutout in the chassis, to ensure correct alignment, and secured with screws and nuts from the Tamiya kit and adhesives as needed.

The shape of the chassis reflects the arrangement of the wheel and casters, while still observing constraints on print size and avoiding wasted material. To conserve bearings, given our finite supply, and knowing the casters would primarily undergo radial forces we friction fit a bearing in the center of each one, which was supported by a cantilevered shaft fixed in the chassis, and prevented from sliding off by a cylindrical end cap. Six pillars support the loading platform to distribute the load more evenly over the chassis. The pillars are printed separately with square pegs that fit into the holes on the platform. Separating these components greatly reduces print times and chances of print failures (since these increases with the number of layers), which is an acceptable trade-off given the relatively loose constraints on the platform and pillar dimensions. Further details about the frame design can be found in Section VII.

II. Numerical Calculations and Results

- $V_{applied} = 6.0\text{V}$, $R_{robot} = 236640\text{rad/m}$
- i estimated $= 2.1\text{A}$
- i actual $= (0.67, 0.49, 0.54)\text{A}$
- T estimated $= 170\text{s}$
- T actual $= (132, 138, 103)\text{s}$
- W_{pmax} estimated $= 45.2\text{kg}$
- W_{pmax} actual $= (14.8, 10.6, 9.12)\text{kg}$

III. Transmission Design

The recommended maximum voltage of 6V was set as our applied voltage. We also determined the temperature-limited maximum current, $i_{max} = \sqrt{\frac{T_{max}-T_{env}}{R_c R_t(1-e^{-1/\tau})t_f}} = 2.1\text{A}$. This value is less than the motor current at maximum mechanical power, $i_{opt} \approx i_{stall}/2 = V_{applied}/2R = 3.6\text{A}$, so it was set as our operating current. And because tow force increased with wheel radius (see Section V), that radius was set to a reasonable upper limit of 50mm. We constructed a simple test gearbox that allowed a measured spur gear stage efficiency of 0.5. The ratio between the third and fourth gears was fixed, as described in Section V. With those values known, the tow force could then be expressed as:

$$F_{tow} = \tau_{wheel}/R_{wheel}$$
$$= \tau_{motor} \cdot R_{planet} \cdot \eta_p^{n_p} \cdot R_{custom} \cdot \eta_c^{n_c} \cdot 1/R_{wheel}$$
$$= k \cdot i \cdot \eta_p^{n_p} \cdot \eta_c^{n_c} \cdot R_{12} \cdot \frac{r_{G4}}{r_{G3} r_{wheel}}$$

The maximum gear ratio was calculated, based on a conservative time limit:

$$\omega_{motor}/R_{max} \cdot r_{wheel} \geq (1\text{m})/(170\text{s})$$
$$\Rightarrow R_{max} = \frac{k(V_{appl} - iR) \cdot r_{wheel}}{(1\text{m})/(170\text{s})}$$

The tow force was plotted as a function of gear ratio between the first and second gears, ending at this calculated maximum point and accounting for gearbox stages as needed (Fig. 2), and the ratio maximizing tow force was chosen.

IV. Power flow

Rio's trial was used for this section as it had the best performance and minimal slipping. Print quality and material availability issues hampered others' trials.

Electrical power in = $V_{applied} \cdot i$

Resistive heating loss = $\frac{i^2}{R}$

Motor frictional heating = $\omega_m \tau_{fric} = (V_{app} - iR)/k \cdot \tau_{fric}$

Motor power out = $P_{in} - P_R - P_{fric}$

Planetary gearbox loss = $P_{m,out} \cdot (1 - \eta_p^{n_p})$

Custom gearbox loss = $P_{p,out} \cdot (1 - \eta_c^{n_c})$.

To calculate rolling resistance, the driven wheel was assumed to bear half of the robot weight and the casters a quarter each. A precise C_{rr} value was difficult to obtain via research, since hot glue was used as the tire material for this trial, so a value of 0.05 was estimated based on industry documentation [1]. For the caster wheels, a value closer to nylon on steel of 0.03 was estimated. $\tau_{rr} = F_N r_{wheel} C_{rr}$, $\theta = \frac{1\text{m}}{r_{wheel}}$, and $U_{lost} = \tau_{rr}\theta$. Rolling resistance power loss = U_{lost}/t_{trial}. This value was calculated for the three wheels, and while it is an ultimately significant power loss, the wheel had to be large due to severe asperities in some of our test surfaces. Bearing power loss in the caster wheels was assumed to be negligible compared to other power losses; bearing power loss in the gearbox is accounted for within measured gear efficiency. The floor frictional heating power was then determined to be the input electrical power, minus these losses. Calculated values are listed in Fig. 3 and input values are listed in Table I.

[1] https://www.mhi.org/media/members/14220/130101690137732025.pdf

Quantity	Value	Units
i	0.617	A
$V_{applied}$	6.0	V
k	0.00247	rad/s
τ_{fric}	0.000523	Nm
R	0.841	Ω
η_p	0.724	unitless
η_c	0.5	unitless
r_{wheel}	13	mm
r_{G1}	8	mm
r_{G3}	9	mm
r_{G4}	46	mm

TABLE I
VALUES USED.

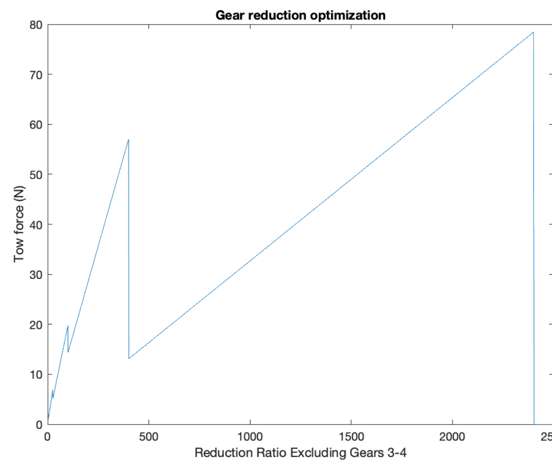

Fig. 2. MATLAB graph used to determine gear ratio.

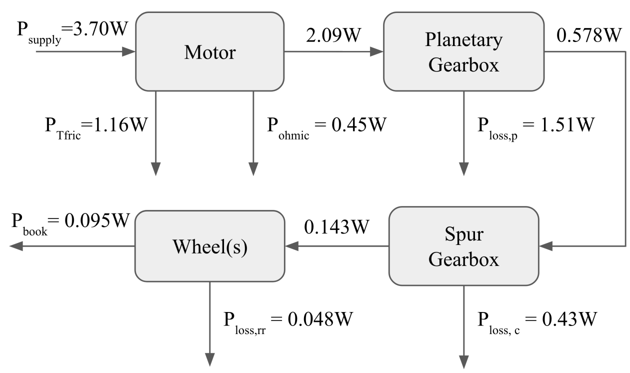

Fig. 3. Power flow. Driven wheel and casters combined for brevity.

V. Component design: Wheel and Gear

Lead: Nick Abram

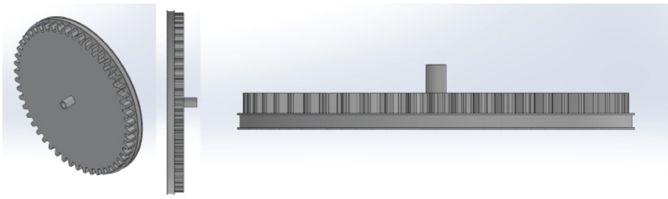

Fig. 4. Three perspective view of Gear 4/Wheel

The Gear 4/Wheel consists of a gear fused with a wheel. The gear has a total of 51 teeth to provide the step up needed to reach a theoretical payload maximum of about 456N. The diametral pitch was chosen to match gear 3 in the gear 2/3 assembly of $10/18\text{mm}$, which was determined by our MATLAB script.

The simplified FBD below (Figure 5) shows that in order to maximize the force of friction, we can do one of four things. First, we can maximize the coefficient of friction μ. Second, we can increase the normal force, which is affected by F_{gear}. Third, Section VI shows how a smaller gear 3 will increase F_{gear}. Fourth, the equations in Figure 5 show that $F_{friction}$ increases as r_{wheel} increases, given a constant margin between the gear and wheel radius. So in order to maximize the reduction and receive the highest F_{gear}, we needed to have the largest gear possible on gear 4 and the smallest gear possible on gear 3, up to the limiting factors of time, space, and wheel radius.

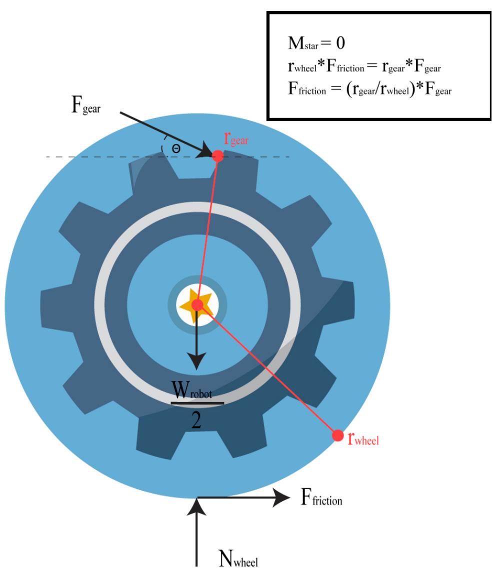

Fig. 5. Simplified FBD of Gear4/Wheel

$$\Sigma F_x = 0 = F_{gear} \cdot cos(\theta) + F_{friction}$$
$$\Sigma F_y = 0 = N_{wheel} - (F_{gear} \cdot sin(\theta) + \frac{W_{robot}}{2})$$
$$\Sigma M_{star} = 0 = F_{gear} \cdot r_{gear} - F_{friction} \cdot r_{wheel}$$

The face width needed to be a minimum of 5 mm to withstand the torques applied to the custom gear; however, we wanted to match the teeth thickness and face width with the other gears, which were determined by the shaft lengths. We circumvented this requirement by fusing the wheel to the gear. Empirical testing as well as 6 showed that this solution worked well. Additionally, this fusion prevented transmission of torque through the shaft.

Lewis Form Factor approximation of face width:

$$width = 16 \cdot T \cdot (\frac{FOS}{S_e}) \cdot (\frac{P^2}{N \cdot (N-11)^{\frac{1}{8}}})$$
$$FOS = 1.7$$
$$width = 5.1\text{mm}$$

The gear face has a small cylindrical tube to constrain axial movement along the shaft. The diameter of the cylinder's hole is 3.2mm to allow a friction fit. The shaft is simply supported by two bearings to provide smooth rotation.

The cylindrical edge of the wheel contains a channel so that a tire material (varying depending on material availability) may be seated in it to increase the coefficient of friction between the wheel and the ground and therefore allow for a greater pulling force before the wheel slips. The channel also prevented the wheel material from slipping from the wheel itself.

We maximized the wheel width given the shaft length and gearbox walls. The reason why we could not pull our specifications is because we assumed coulomb friction on the rubber band. The frictional coefficient between soft rubber and dry wood is about 0.95.[2] When looking at the friction further, the force involves F_{AD}, or the force dependent on the area of real contact.[3] Because of this area dependence, our thin tire meant we were not able to increase the frictional force solely by adding more load to the robot.

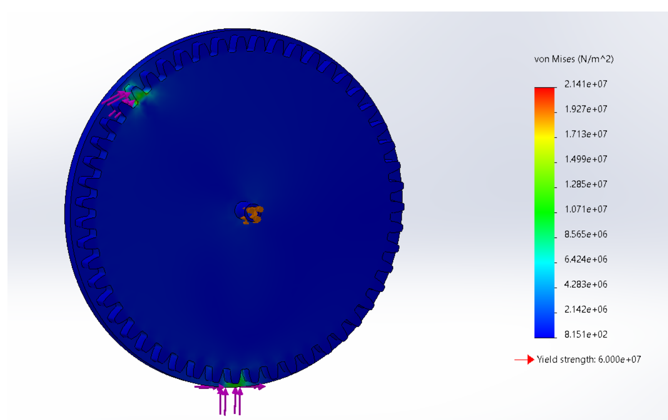

Fig. 6. FEA results for static stress on wheel gear

As Figure 6 shows, the stresses that the wheel gear experience are well within the factor of safety.

[2]https://mae.ufl.edu/designlab/Class%20Projects/Background%20 Information/Friction%20coefficients.htm

[3]https://aip.scitation.org/doi/10.1063/1.5037136

VI. Component design: Intermediate Gears

Lead: Rio Hall-Zazueta

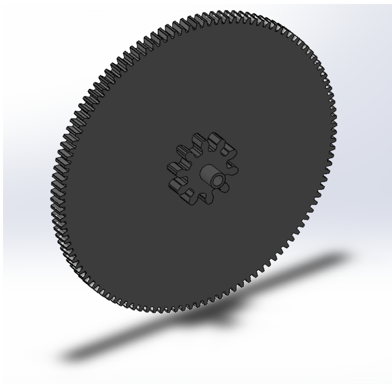

Fig. 7. CAD model of gear 2/3.

The intermediate gear piece consists of two fused gears which connect the stages of the custom gear box, and are printed together to prevent transmission of torque through the shaft (see Fig. 7). Values for diametral pitch, number of teeth and face width were prescribed through gear efficiency testing and consideration of the relative forces on the gear teeth. The cylindrical feature on the front of the component is a spacer, which we included to help prevent axial translation of the gear within the gearbox.

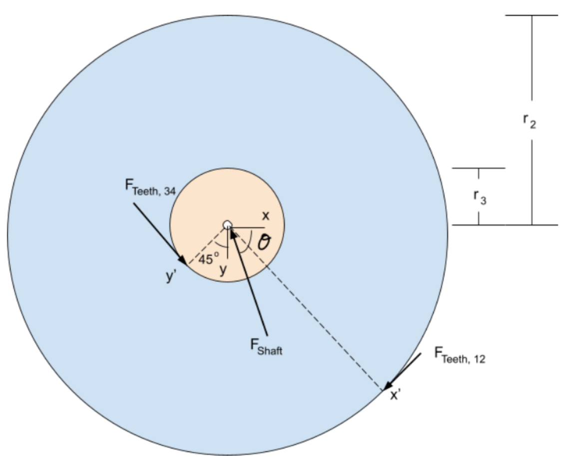

Fig. 8. FBD of intermediate gears 2 and 3

Since the moment at the shaft can be accounted for by measured efficiency values, it is not directly considered in the FBD analysis.The force on the gear teeth from the meshed gears can be approximated as tangential for the purposes of this analysis, since the actual angle of the force relative to the tangent is small. Referring to Fig. 8:

$\Sigma M_{@shaft} = 0 = F_{teeth,34} r_3 - F_{teeth,12} r_2$

$F_{teeth,34} = \frac{r_2}{r_3} F_{teeth,12}$

From similar analysis of gear 1, the following equation can be determined:

$F_{teeth,12} = \frac{1}{r_1} \tau_m R_{GB} \eta_{GB}$, where $\tau_m = ki - \tau_{fric}$

Modifying these force equations with the experimentally determined value of the custom gear efficiency to account for shaft torque:

$F_{teeth,12} = \frac{1}{r_1}(ki - \tau_{fric}) R_{GB} \eta_{GB} \eta_{custom} = 32.1\text{N}$

$F_{teeth,34} = \eta_{custom} \frac{r_2}{r_3} F_{teeth,12} = 81.9\text{N}$

From the gears topic reading, for a gear tooth, $S'_e \approx 4\frac{P^2 F_t r}{wNY}$, for $N \geq 12$. $S'_e = 16\frac{P^2 F_t r}{wN(N-11)^{1/8}}$,

For gear 2 $S'_e \approx 44.4\text{MPa}$, which gives a factor of safety of 1.35.

For gear 3 $S'_e \approx 136.3\text{MPa}$, which gives a factor of safety of 0.44.

This is an acceptable factor of safety for gear 2, but gear 3 appears likely to fail from this analysis. However, this analysis fails to take into account the additional support provided to gear 3 from its contact with gear 2. To account for this the situation is modeled with a static stress FEA.

The FEA predicts a maximum stress of 35.68MPa at the base of the tooth on gear 3. This stress gives a factor of safety of 1.35 accounting for the 0.8 multiplier for fatigue stress. This is a reasonable value for the factor of safety to make failure from the gears unlikely during a relatively short testing time span.

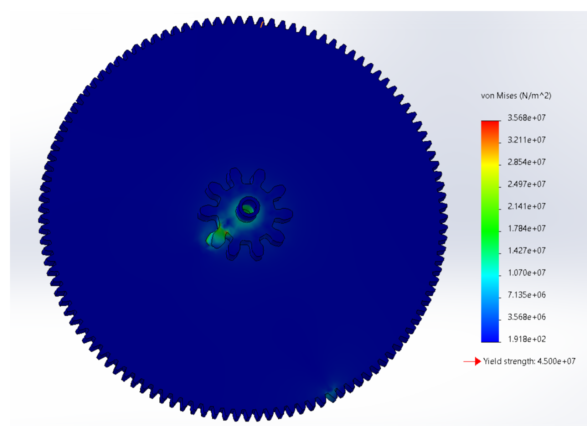

Fig. 9. FEA results for static stress on intermediate gears

Quantity	Value	Units
r_1	0.008	m
r_2	0.046	m
r_3	0.009	m
i	2.102	A
R_{GB}	400	-
η_{GB}	0.275	-
η_{custom}	0.5	-
P_2	1250	m^{-1}
P_3	555.6	m^{-1}
w	0.004	m
N_2	116	-
N_3	10	-
S'_e	60	MPa
Y_{10}	0.167	-

TABLE II

Values used.

VII. Component design: Frame

Lead: Andrew Zerbe

High factors of safety were prioritized in the frame design; a failure of a frame component would necessitate a very long re-print, since they are relatively large. We assumed relative parity between the coefficients of friction of our tire and the book, meaning that the robot would need to support the payload weight; this predicted payload weight of 456N was used as the load weight in our analysis. FBDs of the components, as shown in Fig. 11, provided mixed results; while each 'pillar' component could be modeled as a two-force member, the platform and chassis were both non-obvious shapes without clear and valid simplifications. For example, ribs were created along the bottom of the chassis to increase its stiffness. An anchoring point was printed on the back of the chassis to allow for easy attachment of the payload. The pillar underwent compressive loading, so buckling was its expected failure mode.

We can model the pillar as hinged at one end (the chassis) and fixed at the other (the platform), ignoring the difficult-to-model adhesive connecting it to the chassis and resulting in a conservative estimate with $C = 2$. Fig. 11b) clearly shows that $F_{pillar} = W_{loading}/6$. The cross-sectional area moment of inertia is $\frac{bh^3}{12}$, the modulus of elasticity of PLA is known, and the pillar has dimensions 10x11x110mm. The critical force can then be calculated as $F_{cr} = \frac{C\pi^2 EI}{L^2} = 5.38$kN, which divided by F_{pillar} yields a factor of safety of 71. The limiting factor on pillar size was ultimately the size that would firmly attach to the platform and glue easily to the chassis.

The pillars are attached to the chassis using an adhesive, primarily to prevent horizontal movement due to vibration. The pillars contain small holes for the optional use of string to apply tension and keep the pillars from splaying outwards under the load. The platform is rectangular in shape with a lip to help prevent the load weighing down the robot from sliding. It is centered over the gearbox and runs the length of the robot to allow the center of mass of the load to be adjusted for stability.

The platform and chassis were analysed mostly through FEA, where the two shaft holes and gearbox mount plate were fixed and the platform surface was evenly loaded with our load weight. The tow force was assumed to be roughly negligible compared to this load weight based on preliminary friction testing. This estimated a factor of safety for the whole assembly on the order of 20. Similarly to the pillars, such a high safety factor was a result of its thick, easily printable walls and straightforward design and assembly, especially when glue was involved (necessitating high surface area).

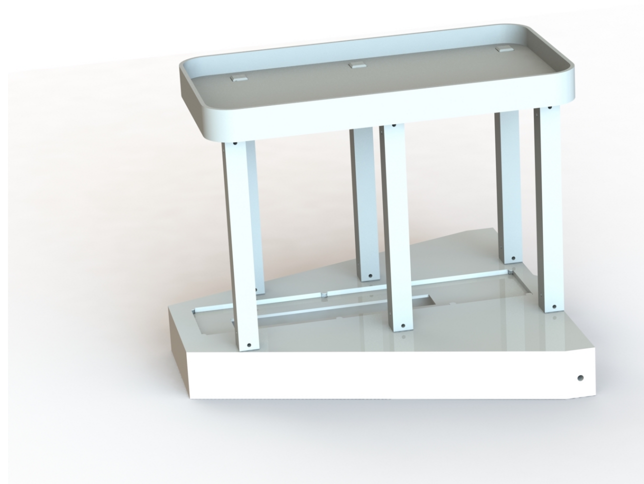

Fig. 10. The frame design.

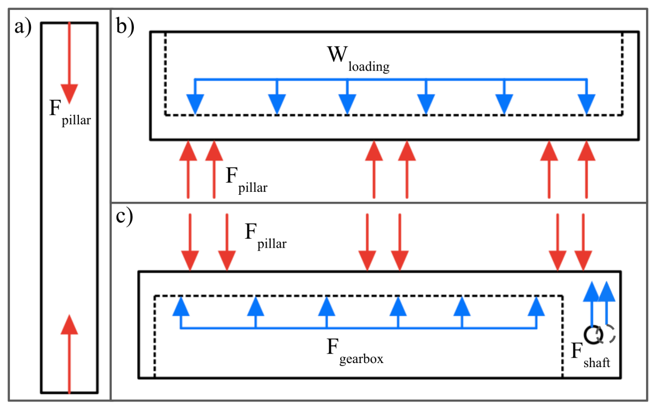

Fig. 11. FBDs of the frame assembly: a) one pillar, b) the platform, and c) the chassis.

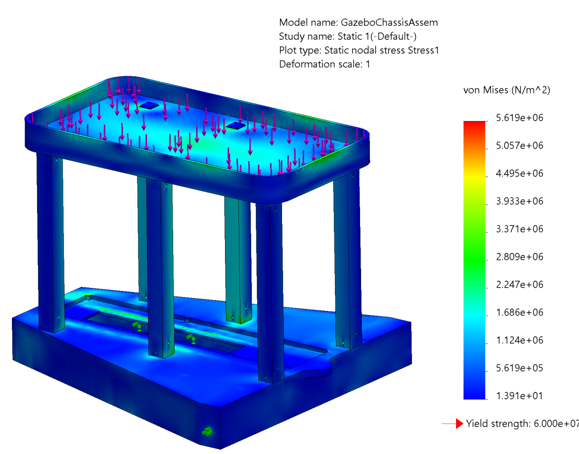

Fig. 12. FEA of the frame assembly.